Unconventional magnetism in the $4d^4$-based $S = 1$ honeycomb system $Ag_3LiRu_2O_6$

R. Kumar,[1] Tusharkanti Dey,[2] P. M. Ette,[3] K. Ramesha,[3] Atasi Chakraborty,[4] I. Dasgupta,[4] J. C. Orain,[5] C. Baines,[5] Sándor Tóth,[6] A. Shahee,[1] S. Kundu,[1] M. Prinz-Zwick,[7] A. A. Gippius,[8,9] N. Büttgen,[7] P. Gegenwart,[2] and A. V. Mahajan[1,*]

[1]*Department of Physics, Indian Institute of Technology Bombay, Powai, Mumbai 400076, India*

[2]*Experimental Physics VI, Center for Electronic Correlations and Magnetism, University of Augsburg, D-86159 Augsburg, Germany*

[3]*Central Electrochemical Research Institute–Madras Unit, CSIR–Madras Complex, Taramani, Chennai 600113, India*

[4]*Department of Solid State Physics, Indian Association for the Cultivation of Science, Jadavpur, Kolkata 700032, India*

[5]*Laboratory for Muon Spin Spectroscopy, Paul Scherrer Insititut (PSI), CH-5232 Villigen, Switzerland*

[6]*Laboratory for Neutron Scattering and Imaging, Paul Scherrer Institute (PSI), CH-5232 Villigen, Switzerland*

[7]*Experimental Physics V, Center for Electronic Correlations and Magnetism, University of Augsburg, D-86159 Augsburg, Germany*

[8]*Department of Physics, M.V. Lomonosov Moscow State University, 199991 Moscow, Russia*

[9]*P.N. Lebedev Physics Institute of Russian Academy of Science, 199991 Moscow, Russia*

(Received 26 June 2017; revised manuscript received 18 January 2019; published 19 February 2019)

We have investigated the thermodynamic and local magnetic properties of the Mott insulating system $Ag_3LiRu_2O_6$ containing Ru^{4+} ($4d^4$) for novel magnetism. The material crystallizes in a monoclinic $C2/m$ structure with RuO_6 octahedra forming an edge-shared two-dimensional honeycomb lattice with limited stacking order along the c direction. The large negative Curie-Weiss temperature ($\theta_{CW} = -57$ K) suggests antiferromagnetic interactions among Ru^{4+} ions, though magnetic susceptibility and heat capacity show no indication of magnetic long-range order down to 1.8 and 0.4 K, respectively. ^{7}Li nuclear magnetic resonance (NMR) shift follows the bulk susceptibility between 120 and 300 K and levels off below 120 K. Together with a power-law behavior in the temperature-dependent spin-lattice relaxation rate between 0.2 and 2 K, it suggest dynamic spin correlations with gapless excitations. Electronic structure calculations suggest an $S = 1$ description of the Ru moments and the possible importance of further neighbor interactions as well as biquadratic and ring-exchange terms in determining the magnetic properties. Analysis of our muon spin rotation data indicates spin freezing below 5 K, but the spins remain on the borderline between static and dynamic magnetism even at 20 mK.

DOI: 10.1103/PhysRevB.99.054417

I. INTRODUCTION

Over the past few years, there has been a shift in focus from $3d$-based systems to the exploration of $4d$- and $5d$-based ones due to the possibility of strong spin-orbit coupling (SOC) driving exotic magnetism [1–15]. The SOC is found to be very strong for $5d$-based systems and could stabilize a Mott insulating state as well as other novel phases [1,2,6,12–15]. Issues such as the realization of the $J_{\text{eff}} = 1/2$ state for the d^5 configuration (half-filled) [2], possible realization of the Kitaev model [16] in d^5 Mott insulators [5,17], and the emergence of spin-liquid states in triangular lattice materials have been widely explored for Ir-based materials [6,7,12,18,19].

However, a very interesting scenario could arise for materials away from half-filling, such as four electrons in the t_{2g} manifold. It has been proposed by Khaliullin [20] that, for oxide systems containing Ru^{4+}, Re^{3+}, Os^{4+}, or Ir^{5+}, there can often be comparable values of SOC ($\lambda \sim 50$–200 meV) and superexchange energy scales ($\frac{4t^2}{U} \sim 50$–100 meV), which could give rise to excitonic magnetism and resultant novel phases. Recently, Meetei *et al.* [21] and Svoboda *et al.* [22] have worked further on this and suggested the possible formation of a spin-orbital liquid even in the absence of geometric frustration. Further, theoretical and experimental attempts have been made to realize this novel magnetism in Ir^{5+}-based perovskite $NaIrO_3$ [23], double perovskites Ba_2YIrO_6 and Sr_2YIrO_6 [24–30], and triple perovskite $Ba_3ZnIr_2O_9$ [31]. However, conclusive evidence of this novel magnetism is still elusive. This implies that one should explore materials with a lower SOC, and Ru^{4+} materials might be a good starting point. Recent theoretical studies also proposed Ru-based materials as good candidates to search for excitonic magnetism [21,22].

In this report, we detail the structural, bulk, and local magnetic properties of the t_{2g}^4-based honeycomb system $Ag_3LiRu_2O_6$ [32] using x-ray diffraction, neutron diffraction, heat capacity, muon spin rotation (μSR) and nuclear magnetic resonance (NMR) techniques. The honeycomb structure decorated with any of the d^4 ions (Ru^{4+}, Re^{3+}, Os^{4+}, and Ir^{5+}) has been proposed to manifest novel physical properties [20]. In $Ag_3LiRu_2O_6$, structurally, Ru atoms give rise to a honeycomb geometry with the Li atom sitting at the center of the honeycomb. Our bulk data do not show any magnetic ordering down to 1.6 K in spite of strong antiferromagnetic interactions. A magnetic contribution to the specific heat is present compared to the nonmagnetic analog $Ag_3LiTi_2O_6$, but without any sharp anomaly. Static susceptibility deduced from the ^{7}Li NMR line shift shows a plateau below 120 K and down to 150 mK. These signatures suggest that the static

*Corresponding author: mahajan@phy.iitb.ac.in

spin correlations are absent or frozen out in the material. The ^{7}Li nuclear spin-lattice relaxation rate $1/T_1$ decreases with decreasing temperature T without any anomaly and displays a power law (T^4) behavior below 2 K. This is suggestive of magnetic moments remaining dynamic and the excitations being gapless. From our μSR measurements, $Ag_3LiRu_2O_9$ presents a spin-glass-like ground state with a transition temperature $T_g = 5.5(5)$ K though the spins display behavior which is at the borderline between static and dynamic even at 20 mK. Our *ab initio* electronic structure calculations indicate negligible SOC and point towards a ferromagnetic coupling between the three nearest neighbors of each Ru and antiferromagnetic further-neighbor couplings. This, coupled with deviations from the Heisenberg model, possibly results in frustration which might drive the observed behavior.

II. EXPERIMENTAL DETAILS

The polycrystalline samples of $Ag_3LiRu_2O_6$ and $Ag_3LiTi_2O_6$ (a nonmagnetic analog used for heat capacity analysis) were prepared in two steps. The precursor Li_2RuO_3 was synthesized by the solid state reaction route by firing stoichiometric amounts of Li_2CO_3 and Ru at 1000 °C for 12 hours in an alumina crucible, followed by another heating cycle at 950 °C for 24 hours after grinding the sample and mixing 10% excess Li_2CO_3. The nonmagnetic Li_2TiO_3 was prepared by firing a stoichiometric mixture of Li_2CO_3 and TiO_2 at 1000 °C. Having obtained single phase samples of the precursors Li_2RuO_3 and Li_2TiO_3, high purity $AgNO_3$ was mixed with each of the starting materials in the ratio 1:10 to prepare the final compositions of $Ag_3LiRu_2O_6$ and $Ag_3LiTi_2O_6$. The crucibles containing the mixture of materials in a 1:10 ratio were slowly heated to 300 °C in air and held at this temperature for 6 hours, followed by cooling to room temperature. The residual $AgNO_3$ and the reaction byproduct $LiNO_3$ were removed by washing the materials with water. X-ray diffraction measurements on the powder samples at room temperature were performed with a Panalytical Xpert Pro diffractometer using Cu-$K\alpha$ radiation. Neutron diffraction data were taken on the DMC beamline at the Paul Scherrer Institute (PSI) at 300 and 1.6 K using a wavelength $\lambda = 2.4586$ Å .

Magnetization M measurements as a function of applied field H (0 to 90 kOe) and temperature T (in the range 1.8 to 400 K)) were performed using a Quantum Design SQUID VSM magnetometer. Zero-field cooled (ZFC) and field cooled (FC) magnetization measurements in a low field of 25 Oe were performed down to 1.8 K. The heat capacity $C_p(T)$ was measured with a Quantum Design physical property measurement system (PPMS) in various applied fields down to about 0.4 K. The μSR experiments were performed on a powder sample at PSI. In the high temperature range ($1.5 < T < 200$ K) we used the General Purpose Surface-muons (GPS) instrument. We mounted about 1 g of sample in a 15 mm × 15 mm Al envelope on a Cu fork. Therefore the sample stops the whole muon beam and we can neglect the experimental background. For the low-temperature regime (20 mK $< T < 17.5$ K) we used the Low Temperature Facility (LTF) instrument. We glued about 1 g of powder with GE varnish on a silver plate to ensure thermal conductivity. Additionally, local probe nuclear magnetic resonance NMR measurements were performed on the ^{7}Li nucleus in a fixed field of 93.95 kOe as also at a fixed frequency of 95 MHz. The variation of line shape with T was measured as was that of the spin-lattice relaxation rate $1/T_1$ down to 150 mK.

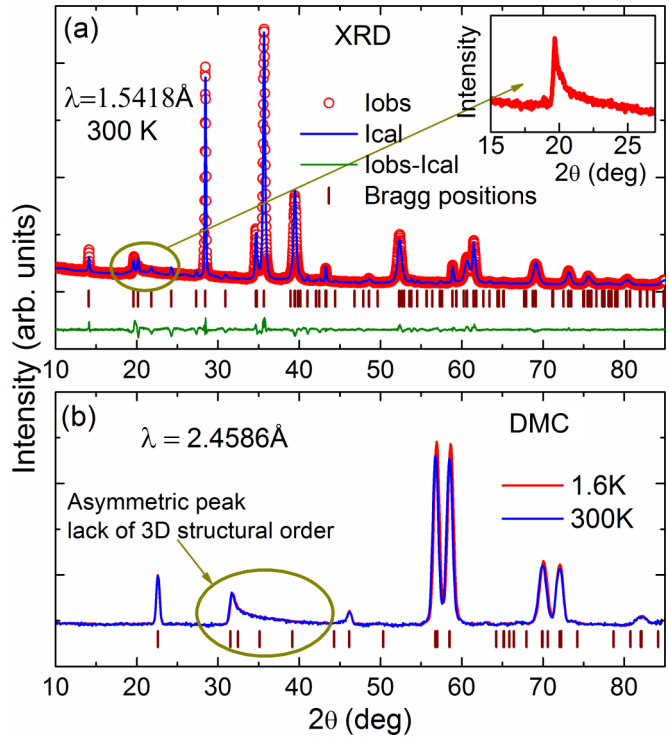

FIG. 1. (a) X-ray diffraction data collected for a powder sample of $Ag_3LiRu_2O_6$ at 300 K. The inset depicts the asymmetric peak (a characteristic of 2D structural order) around 20°. (b) Neutron diffraction data at 300 K (violet solid line) and 1.6 K (cyan solid line) with $\lambda = 2.4586$ Å. The encircled peak (dark yellow) at Bragg angle 31.5° is the asymmetric peak.

III. RESULTS

A. XRD and structural details

The diffraction patterns in Fig. 1 show a sawtooth shaped peak at low angles [see inset of Fig. 1(a) for x-ray data and Fig. 1(b) for neutron diffraction data] which is commonly known as the Warren peak and is characteristic of two-dimensional (2D) structural order with stacking faults in the c direction [33]. Note that stacking faults are not uncommon in such systems, for instance in Na_2IrO_3 [4], Li_2RhO_3 [34], as well as α-$RuCl_3$ [35]. This is not likely to affect the two-dimensional magnetic properties. The neutron diffraction data do not evidence the appearance of additional Bragg peaks down to 1.6 K. Further, absence of magnetic long-range order (LRO) in $Ag_3LiRu_2O_6$ is not due to stacking faults, as we have, in fact, observed LRO in the structurally analogous $Ag_3LiMn_2O_6$ [36]. The x-ray diffraction pattern of $Ag_3LiRu_2O_6$ could be successfully indexed with the monoclinic structure under space group $C2/m$ (space group no. 12), $Z = 2$; and the Rietveld refinement of the x-ray diffraction data with the FULLPROF suite [37] yields the profile parameters $R_{wp} = 4.66\%$, $R_{exp} = 2.72\%$, $R_p = 3.46\%$, and $\chi^2 = 2.93$. The obtained lattice parameters $a = 5.2248(9)$ Å, $b = 9.0459(15)$ Å, $c = 6.5101(12)$ Å, and $\beta = 74.480(12)^\circ$

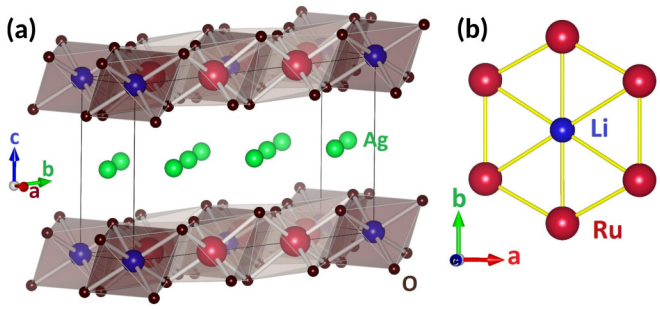

FIG. 2. (a) A unit cell of $Ag_3LiRu_2O_6$ with RuO_6 (Ru shown as pink balls) and LiO_6 (Li shown as blue balls) octahedra in the crystallographic *a*-*b* plane. (b) A depiction of 2D edge sharing honeycomb lattice formed by Ru atoms in the *a*-*b* plane with a Li atom sitting at the center of the honeycomb.

are in excellent agreement with the previously reported results [32]. In $Ag_3LiRu_2O_6$, Ru/Li ions coordinate with eight surrounding oxygen atoms and make RuO_6/LiO_6 octahedra [see Fig. 2(a)]. The RuO_6 octahedra connect in an edge-sharing fashion and give rise to a honeycomb network, and the Ru ions are best viewed as forming a two-dimensional (2D) honeycomb lattice in the *a*-*b* plane [see Fig. 2(b)]. Note that although there is a unique Ru site, there are inequivalent O sites. As a result, there are two types of Ru-O-Ru bonds between a Ru and its three nearest neighbor Ru. As seen later, this results in two different couplings between a Ru and its nearest neighbors. The incorporation of Ag atoms into the primary material Li_2RuO_3 actually works as an intercalation between the Ru layers and essentially makes $Ag_3LiRu_2O_6$ a 2D system.

B. Magnetization

Figure 3 shows the dc susceptibility $\chi(T)$ of $Ag_3LiRu_2O_6$ measured in the T range 2–600 K on a Quantum Design

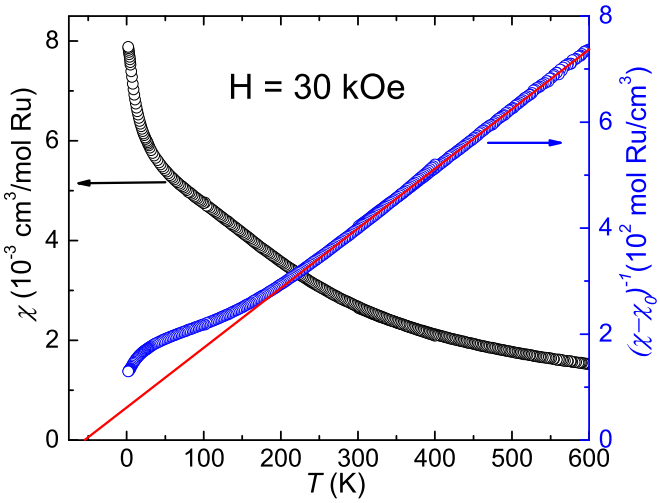

FIG. 3. Variation of susceptibility (left *y* axis) and inverse susceptibility (right *y* axis) for $Ag_3LiRu_2O_6$ with T in the range 2–600 K. The red solid line through the inverse susceptibility data intercepts the temperature axis around −57 K.

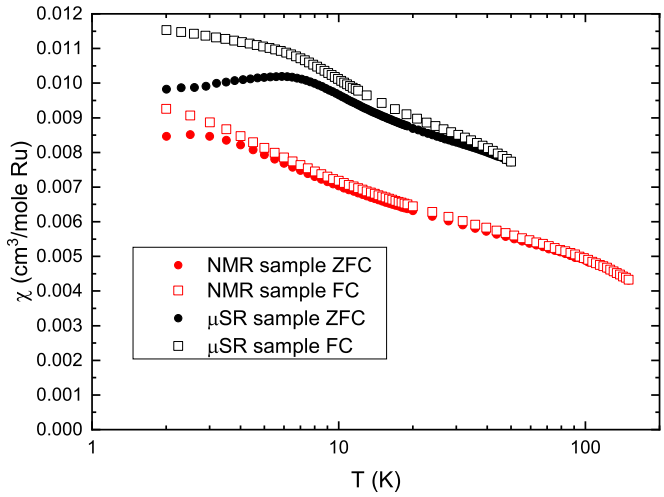

FIG. 4. $\chi = M/H$ measured in an applied field of 25 Oe is shown as a function of T. "NMR sample" refers to the one on which all the measurements were done. Neutron diffraction and μSR measurements were done on the "μSR sample."

magnetic property measurement system (MPMS) with the oven option. The $\chi(T)$ data do not exhibit any anomaly in the T range 2–600 K, though there are hints of a plateau around 100 K. Our neutron diffraction data, see Fig. 1(b), collected down to 1.6 K with wavelength $\lambda = 2.4586$ Å do not show any evidence of a phase transition either. A fit of the data to the Curie-Weiss law ($\chi = \chi_0 + \frac{C}{T-\theta_{CW}}$) in the T range 300–600 K gives $\chi_0 = 1.7 \times 10^{-4}$ cm^3/mol Ru and the asymptotic Curie-Weiss temperature $\theta_{CW} = -57$ K. The negative θ_{CW} indicates the presence of antiferromagnetic coupling between Ru moments. Note that if χ_0 is not left as a free parameter but fixed to a larger value, it yields a smaller θ_{CW} and a smaller Curie constant, though with a poorer fit. Measurements to even higher temperatures would have helped us obtain χ_0 with better accuracy, but the sample degrades at higher temperatures. The value of the Curie constant C is about 0.88 cm^3 K/ mol Ru. This leads to an effective moment of $2.65\mu_B$ which is slightly smaller than the expected spin-only value (for $S = 1$) of $2.83\mu_B$. Magnetization under zero-field cooled (ZFC) and field cooled (FC) conditions was measured in a low field of 25 Oe. This is shown in Fig. 4. We find that there is a weak ZFC-FC bifurcation below about 3 K. In another sample of $Ag_3LiRu_2O_6$ (from a different batch) on which detailed μSR measurements (as well as neutron diffraction) were performed, the bifurcation is greater, and also occurred at a higher temperature of about 6 K. This could arise from a fraction of moments in the sample (extrinsic or intrinsic) which freeze.

C. Heat capacity

Heat capacity measurements were made to probe low-energy excitations associated with possible magnetism in the sample. Using data taken in a larger temperature range, Fig. 5(a) depicts the heat capacity data (C_p) of $Ag_3LiRu_2O_6$ and structurally identical (nonmagnetic) $Ag_3LiTi_2O_6$ in the temperature range 0.4–40 K. The measured heat capacity for $Ag_3LiRu_2O_6$ does not show any significant dependence

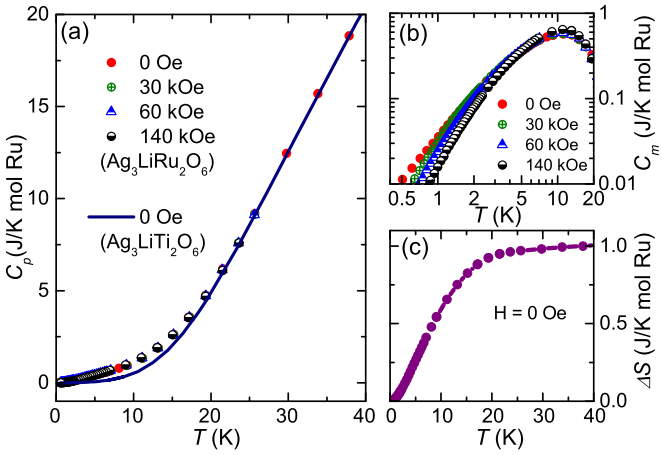

FIG. 5. (a) Heat capacity for $Ag_3LiRu_2O_6$ at different fields (various symbols) and for nonmagnetic analog $Ag_3LiTi_2O_6$ at zero field (solid line) are shown as functions of temperature. (b) Magnetic specific heat C_m as a function of T for $Ag_3LiRu_2O_6$ with $H = 0$, 30, 60, and 140 kOe. (d) Entropy change at $H = 0$ Oe for $Ag_3LiRu_2O_6$.

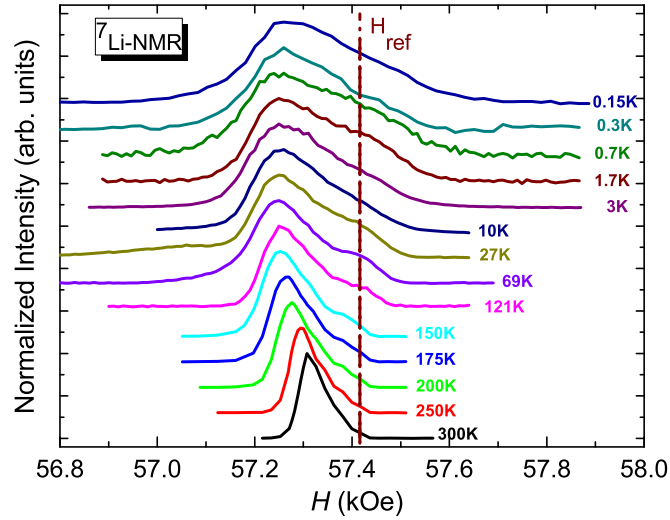

FIG. 6. T dependence of ^{7}Li NMR (normalized) spectra for $Ag_3LiRu_2O_6$ is shown. The shift is seen to be temperature independent from 120 K down to about 150 mK. Note that the spectra above 121 K were actually obtained from the echo integral at various frequencies in a fixed field of 93.94 kOe. For these spectra, the x axis was then converted to field units to compare with the lower temperature data which were obtained by sweeping the field at a fixed frequency of 95 MHz.

on the magnetic field and remains featureless in the measured T range. To extract the magnetic specific heat C_m of $Ag_3LiRu_2O_6$ a procedure similar to that in Ref. [38] was employed. The heat capacity of nonmagnetic $Ag_3LiTi_2O_6$ was measured. The ratio of the Debye temperatures of the Ru compound and the Ti compound, $\frac{\theta_D(\mathrm{Ru})}{\theta_D(\mathrm{Ti})}$, was determined using the procedure of Ref. [38]. The temperature data of $Ag_3LiTi_2O_6$ was multiplied by the ratio of the Debye temperatures ($\frac{\theta_D(\mathrm{Ru})}{\theta_D(\mathrm{Ti})} = 0.95$) before the specific heat of $Ag_3LiTi_2O_6$ was subtracted from the total specific heat of $Ag_3LiRu_2O_6$. The magnetic specific heat C_m thus obtained is shown in Fig. 5(b). At low T, a power-law behavior is seen with an exponent of about 1.65 in zero applied field. The calculated entropy change ($\triangle S$) for $Ag_3LiRu_2O_6$, shown in Fig. 5(c), is estimated to be about 11% of 9.12 J/K mol Ru expected for $S = 1$. The power-law T dependence of C_m and the large quenching of $\triangle S$ supports the realization of a highly degenerate ground state, which is presumably gapless.

D. ^{7}Li NMR

NMR, being a local probe, is instrumental in identifying the change in magnetization at a local level. We performed ^{7}Li (nuclear spin $I = \frac{3}{2}$, gyromagnetic ratio $\frac{\gamma}{2\pi} = 16.546$ MHz/T) NMR spectra measurements (echo integral at variable frequency) at various temperatures from 300 down to 150 mK. Data were obtained in two ways: (i) in a fixed field of $H =$ 93.954 kOe the echo integral was obtained as a function of frequency in the temperature range 300 to 80 K, and (ii) at a fixed frequency of 95 MHz the echo integral was obtained as a function of the field in the T range 120 to 150 mK. The spectra are displayed together in Fig. 6 after scaling the x axis of the frequency sweep data with the gyromagnetic ratio of ^{7}Li to obtain it in field units corresponding to the frequency of the field sweep measurements. The ^{7}Li NMR spectra were found to be asymmetric throughout the measured temperature range, having (i) a main peak, which qualitatively displays a variation with temperature, and (ii) a shoulder on the higher field side which is centered around the zero-shift position, and which remains almost unaffected in the entire temperature range (see Fig. 6). The appearance of this shoulder in ^{7}Li NMR powder spectra is most likely due to the anisotropy of the hyperfine field. Any significant Li/Ru antisite structural disorder is ruled out by our x-ray analysis. In the light of this anisotropy, the static susceptibility was estimated by extracting the K_{iso} (powder averaged line shift) as a function of T by matching the experimental ^{7}Li NMR spectra with the simulated one. The K_{iso} follows the bulk susceptibility data, suggestive of a significant hyperfine coupling between Ru and Li atoms. The K_{iso} becomes nearly T independent (or perhaps weakly decreases) below about 120 K as seen in Fig. 7(a). So the low-temperature rise in the bulk susceptibility appears to be driven by some extrinsic Curie contributions. A finite shift at the lowest temperature suggests gapless spin excitations. Note, however, that NMR measurements are made in a magnetic field and a finite shift could result from the closing of the gap due to the field, but the zero-field heat capacity data exclude the possibility of a gap. The width of the spectrum remains unchanged below $T \approx$ 2 K (see Fig. 6). The hyperfine coupling constant A_{hf} follows the relation $K_{\mathrm{iso}} = K_{\mathrm{chem}} + \frac{A_{hf}}{N_A \mu_B} \chi_{\mathrm{spin}}$ (K_{chem} is the chemical shift, N_A is the Avogadro number, μ_B is the Bohr magneton, and χ_{spin} is the bulk susceptibility). From the slope of the K_{iso} vs χ_{spin} plot, A_{hf} was found to be 2.34(13) kOe/μ_B with $K_{\mathrm{chem}} = 0.03(1)\%$, as shown in the inset of Fig. 7(a). Thevalue of the hyperfine coupling will turn out somewhat larger if the fitting range is limited to higher temperatures.

The ^{7}Li NMR spin-lattice relaxation rate ($1/T_1$) measurements were performed with the saturation recovery method to study the low-energy spin dynamics or to probe the

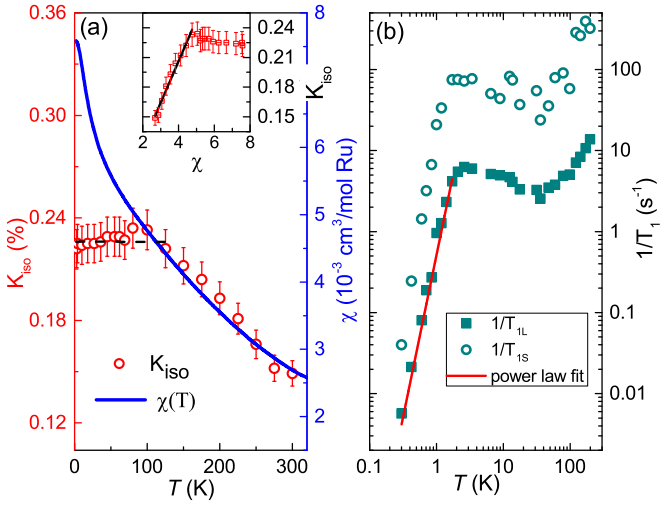

FIG. 7. (a) ^{7}Li NMR line shift (K_{iso}) and the bulk susceptibility (χ) are plotted as functions of temperature, on the left and right axes, respectively. The inset illustrates the ^{7}Li NMR line shift plotted against the bulk magnetic susceptibility (χ) with temperature as an implicit parameter. (b) ^{7}Li nuclear spin-lattice relaxation rate plotted against temperature. The solid line is a power-law fit of the $1/T_{1L}$ data, yielding a T^4 variation.

q-averaged dynamical susceptibility of $Ag_3LiRu_2O_6$ in the temperature range 0.3–210 K at a transmitter frequency of 95 MHz ($H \simeq 57.3$ kOe). The recovery of the longitudinal ^{7}Li nuclear magnetization was monitored after a saturating pulse sequence, and the data in the low-temperature regime are shown in Fig. 8. The recovery of the longitudinal magnetisation $m(t)$ was fit to $1 - \frac{m(t)}{m(\infty)} = A\exp(-t/T_{1L}) + B\exp(-t/T_{1S})$, where T_{1L}, T_{1S} are the long and short components of the relaxation time and A and B are constants. The short component (T_{1S}) likely corresponds to an initial fast relaxation associated with spectral diffusion due to incomplete saturation of the broad line. The long component (T_{1L}) is expected to be the intrinsic contribution. However, both the

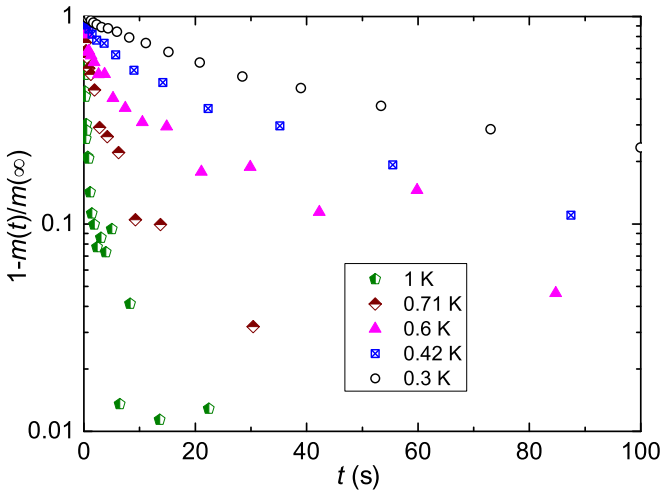

FIG. 8. Recovery of the longitudinal ^{7}Li nuclear magnetization $m(t)$ plotted as $1 - m(t)/m(\infty)$ versus the time delay t at various temperatures.

long and the short T_1 components follow the same qualitative behavior. Figure 7(b) illustrates the variation of $1/T_{1L}$ and $1/T_{1S}$ in the T range 0.3–210 K. A gradual decrease is seen down to 30 K with a broad plateau around 2 K which is followed by a falloff with a T^4 power law at lower T. The broad maximum is not due to any spin freezing, as the ^{7}Li NMR line remains unbroadened all the way from 120 K down to 150 mK. The T^4 variation of $1/T_1$ below 2 K suggests that the spins remain dynamic and that the excitations are gapless. The data could be fit to a gapped behavior with a gap of about 3 K but our heat capacity data show a power-law decrease. Such power-law behavior is also seen in other spin-liquid candidate materials [12,39].

E. μSR

As mentioned before, for the GPS experiments, the background signal can be neglected. For the LTF data (20 mK $< T <$ 17.5 K) we need to estimate the background signal Bgd. At 3 K, we have data from the GPS as well as the LTF beamlines. We then vary Bgd for the LTF data so that the background subtracted data for LTF (at 3 K) coincides with the GPS data at 3 K. This yields Bgd = 0.014(1). For clarity, and to directly compare the GPS and LTF data, the raw curves are presented in terms of polarization, $P(t)$, where

$$P(t) = \frac{A(t) - \text{Bgd}}{A_0 - \text{Bgd}}. \tag{1}$$

We present first the zero-field (ZF) experiments that we have performed from 200 K down to 20 mK (Fig. 9 left). From these data, it is clear that there is a transition in the whole compound between 20 K and 1.56 K. Indeed, at high temperature, in the paramagnetic regime, the depolarization is quite slow and can be attributed to the influence of Li magnetic nuclei. We assumed that the depolarization at 200 K is of a Gaussian form due to static nuclear moments. We then fitted the 200 K data data with a Kubo-Toyabe function [40,41]:

$$P_{200\,\text{K}}(t) = \tfrac{1}{3} + \tfrac{2}{3}[1 - (\sigma_{\text{Nucl}}t)^2]e^{-\frac{1}{2}(\sigma_{\text{Nucl}}t)^2}. \tag{2}$$

This yields $\sigma_{\text{Nucl}} = 0.156(1)\ \mu\text{s}^{-1}$ which is directly linked to the nuclear field H_{Nucl} via $\sigma_{\text{Nucl}} = \gamma_\mu H_{\text{Nucl}}$, where $\gamma_\mu = 2\pi \times 135.5\ \mu\text{s T}^{-1}$ is the gyromagnetic factor of the muons. We found $H_{\text{Nucl}} = 1.83(2)$ G, which is in the usual range of nuclear field values.

At low temperatures, the depolarization is rather quick, on the 0.1 μs scale, and the depolarization at long time is close to 1/3. This is characteristic of frozen or quasistatic magnetism. Nevertheless, the lack of spontaneous oscillations could be directly linked to an absence of long range ordered magnetism. Therefore, our μSR experiment reveals a short range ordered spin-glass-like ground state or a dynamic ground state with a large distribution of fields. To have better insight on the ground state probed by μSR, we fitted the data with an equation containing two relaxing components which has been used for other spin-glass systems [42,43]:

$$P(t) = f_{\text{Fro}}\left(\tfrac{2}{3}e^{-\lambda_{\text{Fast}}t} + \tfrac{1}{3}e^{-\lambda t}\right) + (1 - f_{\text{Fro}})P_{200\,\text{K}}e^{-\lambda t}, \tag{3}$$

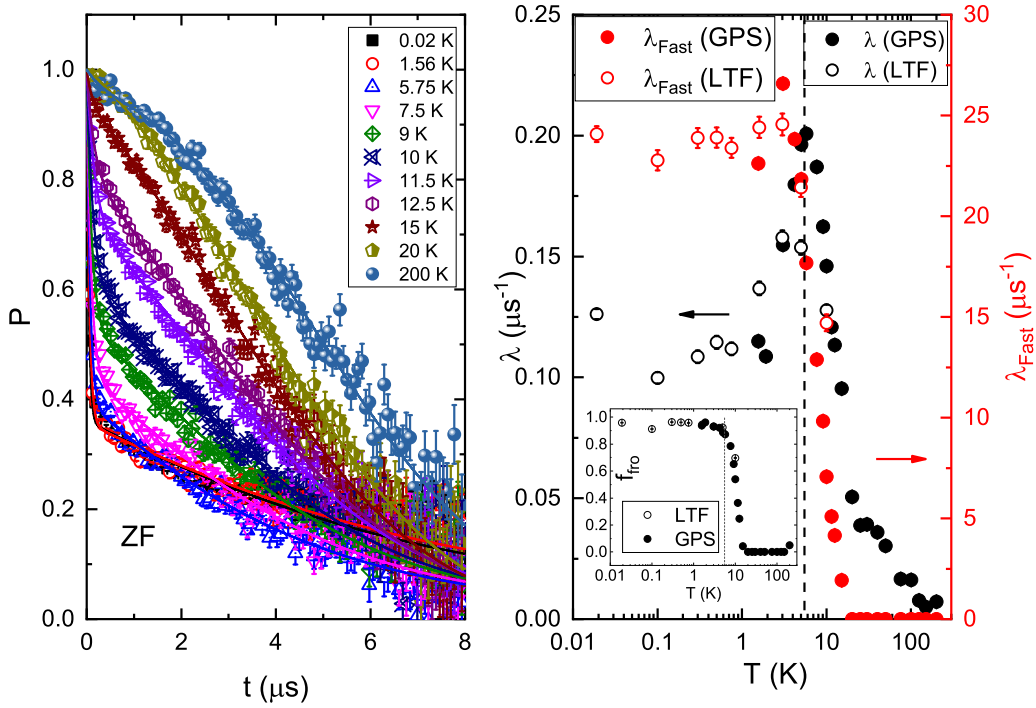

FIG. 9. Left: Polarization versus time at selected temperatures in zero field. The circles are the raw data and the lines are the fit with Eq. (3). Right: Depolarization rates versus temperature. The black circles are λ (left scale) and the red ones are λ_{Fast} (right scale). Inset: Frozen fraction versus temperature. The solid circles are the GPS results, the open circles are the LTF results. The dashed line represents the transition temperature T_g.

where f_{Fro} is the fraction of sample in the frozen state, λ_{Fast} accounts for the fast depolarization at short time and represents the distribution of quasistatic fields in the sample, and λ accounts for the electronic magnetism and could be linked to its fluctuations. Note that we also tried to fit the data using the dedicated spin glass function [44] as well as dynamic and static Kubo-Toyabe functions, which resulted in poorer fits than with Eq. (3).

The results are presented in Fig. 9 right. The small differences between GPS and LTF likely arise from the difficulty to fully characterize Bgd in LTF. The frozen fraction increases at 10 K, getting close to 1 below 3 K. Therefore, the transition is not due to an impurity but presents a bulk character. Further, from the depolarization rate λ we can determine the transition temperature T_g. Indeed, λ possesses a peak around 5.5(5) K, which is characteristic of a transition to frozen magnetism. Moreover, there is a very small plateau at 0.11(1) μs^{-1} which could be related to small fluctuations of the magnetism below 1 K and could be due to a quasistatic order. Further, below this temperature, λ_{Fast} presents a plateau around 25(2) μs^{-1} which is due to the distribution of the quasistatic fields. From this value, one can directly compute the field distribution $\Delta = \lambda_{Fast}/\gamma_\mu = 290(30)$ G.

To distinguish between static and dynamic magnetism we applied several longitudinal fields in the direction of the muon beam. Indeed, in the case of static magnetism a longitudinal field which is 10 times the field distribution should decouple the muons, whereas in the dynamic case a longitudinal field 50 times stronger than the field distribution is needed [45]. At 20 mK, the muons are almost fully decoupled under a field of 0.5 T (∼17 × Δ) (Fig. 10) indicating that the magnetism observed below 5 K is at the borderline between static and dynamic behavior. Therefore, due to the lack of spontaneous oscillations and the decoupling experiment, $Ag_3LiRu_2O_6$ presents a spin-glass-like ground state with a transition temperature $T_g = 5.5(5)$ K based on the μSR analysis.

F. Electronic structure calculations

In order to obtain further insight into the possible origin of the observed magnetic behavior, given the apparent absence

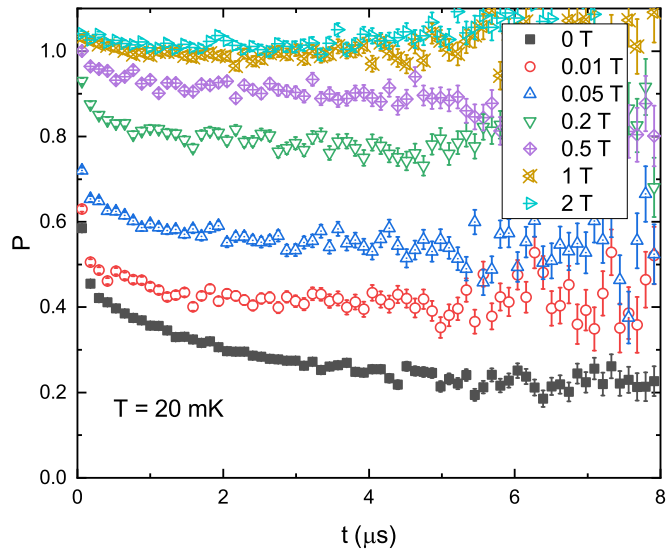

FIG. 10. Muon polarization versus time at 20 mK with different applied fields.

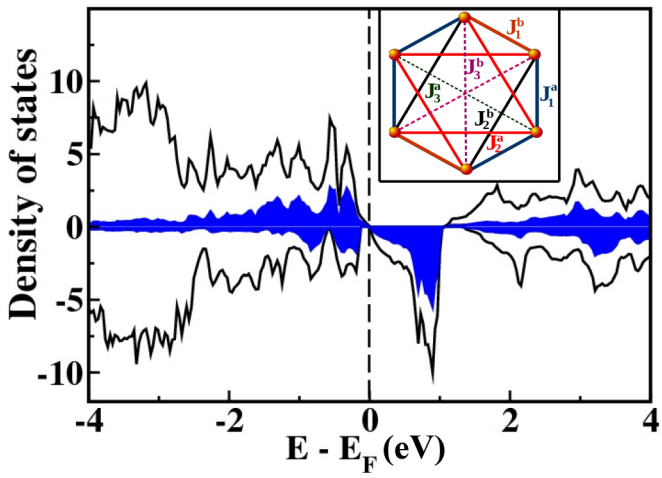

FIG. 11. Spin polarized (ferromagnetic configuration) total and Ru projected density of states in units of states per eV per formula unit (blue shaded area) for $Ag_3LiRu_2O_6$. The exchange paths and the various exchange interactions are shown in the inset.

of geometric frustration, we have carried out electronic structure calculations using the full-potential linearized augmented plane wave (FP-LAPW) [46,47] plus local orbitals method using the WIEN2K code [48]. Exchange and correlation effects are treated within generalized gradient approximation (GGA) [49] of Perdew, Burke, and Ernzerhof including Hubbard U [50] and spin-orbit coupling (SOC). The double counting correction in the GGA+U formalism is taken into account around the mean field approximation [51]. The calculations were done with usual values of U and J_H [52] chosen for Ru: $U = 3.0$ eV and Hund's coupling $J_H = 0.7$ eV. The calculations were also checked for various other values of U. In order to achieve the convergence of energy eigenvalues, the kinetic energy cutoff was chosen to be $K_{max}R_{MT} = 7.0$, where R_{MT} denotes the smallest atomic sphere radius and K_{max} gives the magnitude of the largest K vector in the plane-wave expansion in the interstitial region. The Brillouin zone integrations were performed with an $8 \times 8 \times 6$ k-points mesh. The total energies necessary for the calculation of symmetric exchange interactions [53] were calculated using density functional theory (DFT) and the projector augmented-wave (PAW) method as encoded in the Vienna *ab initio* simulation package (VASP). The kinetic energy cutoff of the plane wave basis was chosen to be 600 eV and a Γ centered $4 \times 4 \times 6$ k mesh has been used for Brillouin zone (BZ) integration.

The spin polarized density of states in the framework of GGA+U with $U = 3.0$ eV and $J_H = 0.7$ eV in the ferromagnetic configuration [54] is shown in Fig. 11. The system is found to be insulating, with the majority Ru t_{2g} spin states completely occupied while the minority t_{2g} states are only partially occupied. The e_g states for both the spin channels are completely empty. As a consequence of the monoclinic distortion promoted by Jahn-Teller active Ru^{4+} ions the degeneracy of the Ru t_{2g} states is completely lifted, which on inclusion of the Hubbard U introduces a gap in the minority spin channel. The total moment is calculated to be $4\mu_B$ (per formula unit) with moments at Ru and O sites being $1.16\mu_B$ and $0.18\mu_B$ respectively, suggesting strong hybridization of the Ru with oxygen states. Next, we included spin-orbit coupling in our calculation. The total moment was then calculated to be $3.97\mu_B$ with spin and orbital moments at the Ru site $1.15\mu_B$ and $0.03\mu_B$, respectively. The small orbital moment suggests that a spin-only description is valid and neither the LS nor the jj coupling schemes should be employed. These calculations suggest that the system is far away from the $J = 0$ limit and the $S = 1$ description of the system is more appropriate. To understand the absence of an ordered state, we calculated the first, second, and third neighbor symmetric exchange interactions, mapping the density functional total energies obtained using the Vienna *ab initio* simulation package (VASP) within the projector-augmented wave (PAW) method onto the Heisenberg model following the method proposed in [53]. The magnitude and the sign of the symmetric exchange interactions are found to be very sensitive to the chosen configuration for calculation and the size of the simulation cell, suggesting the importance of the higher order magnetic interactions (biquadratic and four-spin ring couplings), as the usual approximation of the Hubbard model reducing to the Heisenberg model in the limit of large U may not be applicable here [55]. The calculations have been done (with the experimental structural parameters) for several spin configurations using simulation cells of different sizes. Our calculations reveal that the nearest-neighbor exchange interactions J_1^a and J_1^b are ferromagnetic while the further-neighbor interactions (such as J_2^a, J_2^b, J_3^a, and J_3^b) are antiferromagnetic. On the other hand, if we relax the structure and then calculate the couplings, the nearest and the next-nearest neighbor interactions turn out to be antiferromagnetic. With a larger number of antiferromagnetic further-neighbour couplings, one can still recover a negative θ_{CW} as observed experimentally. This, coupled with the ring exchange and biquadratic couplings, introduces frustration in the system and possibly drives the system away from order.

IV. DISCUSSION

From the wide range of measurements that we have presented together with first-principles electronic structure calculations, let us now look at things in perspective. Usual bulk susceptibility measurements did not show any signatures of long-range order down to 1.8 K. Heat capacity measurements (zero or nonzero applied field) also do not evidence any peak down to 0.4 K. ^{7}Li NMR measurements on the same sample did not show any line broadening nor any peak in the spin lattice relaxation rate down to 0.15 K. In fact, the ^{7}Li shift (which probes the intrinsic susceptibility), starting at room temperature, increases with decreasing temperature. This suggests that there is magnetism in the system which must come from Ru^{4+} ions ($4d^4$). Note that we tried to fit the T variation of the intrinsic susceptibility to the formula given by Kotani [56] for the Van Vleck susceptibility of d^4 systems. This gave rise to very poor fits. The apparent agreement with the Kotani formula for the susceptibility of $Ag_3LiRu_2O_6$ in Ref. [57] is misleading, as that work seems to have considered only the T region where the susceptibility is nearly constant. Also, our calculations suggest that this is a spin-only moment. With a continued decrease in temperature, the ^{7}Li shift levels off below about 120 K and remains so

down to 150 mK. The ^{7}Li NMR linewidth does not show any divergence either, and remains constant down to 150 mK. All the above suggests that the magnetism in this system somehow gets quenched below 120 K and no order sets in. Note that the NMR measurements are in a field of about 57 kOe, which corresponds to a significant energy scale in our low-T regime (below 5 K or so). Let us now look at the results of low- and zero-field measurements. The magnetic heat capacity shows no special features other than a power-law variation at low T (below about 4 K) and a broad maximum around 10 K. The low-field (25 Oe) ZFC and FC magnetizations do show some bifurcation at low T which is sample dependent. The sample on which we performed the heat capacity and all the NMR measurements showed a weak ZFC-FC bifurcation (less than 10%) below about 3 K. When the same sample was measured in μSR (zero field), we found evidence of freezing around 3.5 K. On the other hand, the sample on which we did detailed μSR measurements (presented here) showed a larger ZFC-FC bifurcation and around 7 K. This sample shows a freezing of moments below about 5.5 K from μSR. The question now is how to reconcile the μSR data with the NMR, susceptibility, and heat capacity data. It appears that the zero-field μSR and low-field magnetization results are consistent with each other. For the zero-field heat capacity, the lack of entropy as well as the broad peak around 10 K and the power-law behavior at low temperatures could perhaps arise in the case of a spin glass state. The differing NMR results might come from a field effect. The ^{7}Li NMR linewidth should have shown a critical divergence (or at least a significant increase) around the freezing temperature. The absence of this suggests that the applied field prevents the formation of static moments. Nevertheless, these results are very similar to the one obtained in another honeycomb compound, Li_2RhO_3 [34]. Note also that the magnetism observed by us in μSR below 5 K is at the borderline of static and dynamic. Therefore, even if the μSR experiments rule out the possibility of a quantum spin-liquid ground state due to the presence of frozen magnetism below 5.5(5) K, this compound does not present a regular spin-glass behavior.

V. CONCLUSIONS

In summary, we investigated the structural, thermodynamic, and local magnetic properties of the honeycomb-structure-based quantum material $Ag_3LiRu_2O_6$ by performing x-ray diffraction, neutron diffraction, susceptibility, heat capacity, and ^{7}Li NMR measurements. The presence of an asymmetric peak in both x-ray and neutron diffraction profiles is suggestive of a 2D structural ordering (honeycomb) in the a-b plane. The $\chi(T)$ data indicate a strong antiferromagnetic coupling between the Ru moments without showing any anomaly down to 2 K, and the neutron diffraction carried out down to 1.6 K does not detect any magnetic order. Heat capacity displays a $\sim T^{1.7}$ dependence at low T, and the deduced entropy change was found to be highly suppressed: $\Delta S \sim 11\%$ of that for an ordered spin-1 system. ^{7}Li NMR powder spectra measurements helped in extracting the intrinsic susceptibility of Ru moments, and a leveling off of the NMR line shift was found for $T \leqslant 120$ K. Our electronic structure calculations provide a clue to the origin of the observed susceptibility saturation in this system, which (in principle) is not geometrically frustrated. Our study suggests that the magnetism here is not excitonic in origin. We propose that the frustration induced by further-neighbor couplings and a deviation from the simple Heisenberg model is responsible for the lack of LRO in this system. While spin freezing below about 5 K is evidenced from our zero-field μSR data, from the longitudinal field decoupling experiments, the moments are at the borderline between static and dynamic even at 20 mK. It needs to be explored whether defects such as stacking faults finally drive the system to a frozen state and whether the pristine system might be a spin liquid.

ACKNOWLEDGMENTS

This work is partially based on experiments performed at the Swiss spallation neutron source SINQ, Paul Scherrer Institute, Villigen, Switzerland. We thank Department of Science and Technology (DST), Government of India for financial support through the BRICS project Helimagnets. R.K. acknowledges Council of Scientific and Industrial Research (CSIR) (India) and IRCC (IIT Bombay) for support via research fellowships to carry out this research work. P.M.E. acknowledges CSIR, INDIA for providing financial support under a CSIR-SRF fellowship (Grant No. 31/52(14)2k17). A.V.M. thanks the Alexander von Humboldt Foundation for support. Work at Augsburg was supported by the Deutsche Forschungsgemeinschaft (DFG) through the collaborative research center TRR80 (Augsburg/Munich). A.A.G. acknowledges the financial support from the RFBR under Grant No. 17-52-80036. We thank Kedar Damle for useful discussions and Dana Vieweg for technical help.

[1] Y. Okamoto, M. Nohara, H. Aruga-Katori, and H. Takagi, Phys. Rev. Lett. **99**, 137207 (2007).

[2] B. J. Kim, H. Ohsumi, T. Komesu, S. Sakai, T. Morita, H. Takagi, and T. Arima, Science **323**, 1329 (2009).

[3] Y. Singh, S. Manni, J. Reuther, T. Berlijn, R. Thomale, W. Ku, S. Trebst, and P. Gegenwart, Phys. Rev. Lett. **108**, 127203 (2012).

[4] S. K. Choi, R. Coldea, A. N. Kolmogorov, T. Lancaster, I. I. Mazin, S. J. Blundell, P. G. Radaelli, Y. Singh, P. Gegenwart, K. R. Choi, S.-W. Cheong, P. J. Baker, C. Stock, and J. Taylor, Phys. Rev. Lett. **108**, 127204 (2012).

[5] T. Takayama, A. Kato, R. Dinnebier, J. Nuss, H. Kono, L. S. I. Veiga, G. Fabbris, D. Haskel, and H. Takagi, Phys. Rev. Lett. **114**, 077202 (2015).

[6] T. Dey, A. V. Mahajan, P. Khuntia, M. Baenitz, B. Koteswararao, and F. C. Chou, Phys. Rev. B **86**, 140405 (2012).

[7] T. Dey, A. V. Mahajan, R. Kumar, B. Koteswararao, F. C. Chou, A. A. Omrani, and H. M. Ronnow, Phys. Rev. B **88**, 134425 (2013).

[8] T. Dey and A. Mahajan, Eur. Phys. J. B **86**, 247 (2013).

[9] R. A. Borzi, S. A. Grigera, J. Farrell, R. S. Perry, S. J. S. Lister, S. L. Lee, D. A. Tennant, Y. Maeno, and A. P. Mackenzie, Science **315**, 214 (2007).

[10] W. Wu, A. McCollam, S. A. Grigera, R. S. Perry, A. P. Mackenzie, and S. R. Julian, Phys. Rev. B **83**, 045106 (2011).

[11] M. A. de Vries, A. C. Mclaughlin, and J.-W. G. Bos, Phys. Rev. Lett. **104**, 177202 (2010).

[12] R. Kumar, D. Sheptyakov, P. Khuntia, K. Rolfs, P. G. Freeman, H. M. Rønnow, T. Dey, M. Baenitz, and A. V. Mahajan, Phys. Rev. B **94**, 174410 (2016).

[13] W. Witczak-Krempa, G. Chen, Y. B. Kim, and L. Balents, Annu. Rev. Condens. Matter Phys. **5**, 57 (2014).

[14] C. M. Thompson, C. A. Marjerrison, A. Z. Sharma, C. R. Wiebe, D. D. Maharaj, G. Sala, R. Flacau, A. M. Hallas, Y. Cai, B. D. Gaulin, G. M. Luke, and J. E. Greedan, Phys. Rev. B **93**, 014431 (2016).

[15] A. E. Taylor, R. Morrow, R. S. Fishman, S. Calder, A. I. Kolesnikov, M. D. Lumsden, P. M. Woodward, and A. D. Christianson, Phys. Rev. B **93**, 220408 (2016).

[16] A. Kitaev, Ann. Phys. **321**, 2 (2006).

[17] G. Jackeli and G. Khaliullin, Phys. Rev. Lett. **102**, 017205 (2009).

[18] A. Catuneanu, J. G. Rau, H.-S. Kim, and H.-Y. Kee, Phys. Rev. B **92**, 165108 (2015).

[19] M. Becker, M. Hermanns, B. Bauer, M. Garst, and S. Trebst, Phys. Rev. B **91**, 155135 (2015).

[20] G. Khaliullin, Phys. Rev. Lett. **111**, 197201 (2013).

[21] O. N. Meetei, W. S. Cole, M. Randeria, and N. Trivedi, Phys. Rev. B **91**, 054412 (2015).

[22] C. Svoboda, M. Randeria, and N. Trivedi, Phys. Rev. B **95**, 014409 (2017).

[23] M. Bremholm, S. E. Dutton, P. W. Stephens, and R. J. Cava, J. Solid State Chem. **184**, 601 (2011).

[24] T. Dey, A. Maljuk, D. V. Efremov, O. Kataeva, S. Gass, C. G. F. Blum, F. Steckel, D. Gruner, T. Ritschel, A. U. B. Wolter, J. Geck, C. Hess, K. Koepernik, J. van den Brink, S. Wurmehl, and B. Büchner, Phys. Rev. B **93**, 014434 (2016).

[25] F. Hammerath, R. Sarkar, S. Kamusella, C. Baines, H.-H. Klauss, T. Dey, A. Maljuk, S. Gaß, A. U. B. Wolter, H.-J. Grafe, S. Wurmehl, and B. Büchner, Phys. Rev. B **96**, 165108 (2017).

[26] Q. Chen, C. Svoboda, Q. Zheng, B. C. Sales, D. G. Mandrus, H. D. Zhou, J.-S. Zhou, D. McComb, M. Randeria, N. Trivedi, and J.-Q. Yan, Phys. Rev. B **96**, 144423 (2017).

[27] G. Cao, T. F. Qi, L. Li, J. Terzic, S. J. Yuan, L. E. DeLong, G. Murthy, and R. K. Kaul, Phys. Rev. Lett. **112**, 056402 (2014).

[28] L. T. Corredor, G. Aslan-Cansever, M. Sturza, K. Manna, A. Maljuk, S. Gass, T. Dey, A. U. B. Wolter, O. Kataeva, A. Zimmermann, M. Geyer, C. G. F. Blum, S. Wurmehl, and B. Büchner, Phys. Rev. B **95**, 064418 (2017).

[29] S. Bhowal, S. Baidya, I. Dasgupta, and T. Saha-Dasgupta, Phys. Rev. B **92**, 121113 (2015).

[30] K. Pajskr, P. Novák, V. Pokorný, J. Kolorenč, R. Arita, and J. Kuneš, Phys. Rev. B **93**, 035129 (2016).

[31] A. Nag, S. Middey, S. Bhowal, S. K. Panda, R. Mathieu, J. C. Orain, F. Bert, P. Mendels, P. G. Freeman, M. Mansson, H. M. Ronnow, M. Telling, P. K. Biswas, D. Sheptyakov, S. D. Kaushik, V. Siruguri, C. Meneghini, D. D. Sarma, I. Dasgupta, and S. Ray, Phys. Rev. Lett. **116**, 097205 (2016).

[32] S. A. J. Kimber, C. D. Ling, D. Jonathan, P. Morris, A. Chemseddine, P. F. Henry, and D. N. Argyriou, J. Mater. Chem. **20**, 8021 (2010).

[33] B. E. Warren, Phys. Rev. **59**, 693 (1941).

[34] P. Khuntia, S. Manni, F. R. Foronda, T. Lancaster, S. J. Blundell, P. Gegenwart, and M. Baenitz, Phys. Rev. B **96**, 094432 (2017).

[35] M. Majumder, M. Schmidt, H. Rosner, A. A. Tsirlin, H. Yasuoka, and M. Baenitz, Phys. Rev. B **91**, 180401 (2015).

[36] R. Kumar (unpublished).

[37] J. Rodriguez-Carvajal, FullProf: A Program for Rietveld Refinement and Profile Matching Analysis of Complex Powder Diffraction Patterns (ILL, unpublished).

[38] M. Bouvier, P. Lethuillier, and D. Schmitt, Phys. Rev. B **43**, 13137 (1991).

[39] T. Dey, M. Majumder, J. C. Orain, A. Senyshyn, M. Prinz-Zwick, S. Bachus, Y. Tokiwa, F. Bert, P. Khuntia, N. Büttgen, A. A. Tsirlin, and P. Gegenwart, Phys. Rev. B **96**, 174411 (2017).

[40] R. S. Hayano, Y. J. Uemura, J. Imazato, N. Nishida, T. Yamazaki, and R. Kubo, Phys. Rev. B **20**, 850 (1979).

[41] R. Kubo, Hyperfine Interact. **8**, 731 (1981).

[42] A. A. Aczel, Z. Zhao, S. Calder, D. T. Adroja, P. J. Baker, and J.-Q. Yan, Phys. Rev. B **93**, 214407 (2016).

[43] H. Guo, K. Manna, H. Luetkens, M. Hoelzel, and A. C. Komarek, Phys. Rev. B **94**, 205128 (2016).

[44] Y. J. Uemura, T. Yamazaki, D. R. Harshman, M. Senba, and E. J. Ansaldo, Phys. Rev. B **31**, 546 (1985).

[45] A. Yaouanc and P. D. de Reotier, *Muon Spin Rotation, Relaxation, and Resonance Applications to Condensed Matter* (Oxford University Press, Oxford, 2011).

[46] G. K. H. Madsen, P. Blaha, K. Schwarz, E. Sjöstedt, and L. Nordström, Phys. Rev. B **64**, 195134 (2001).

[47] K. Schwarz, P. Blaha, and G. K. H. Madsen, Comput. Phys. Commun. **147**, 71 (2002).

[48] P. Blaha, K. Schwarz, G. K. H. Madsen, D. Kvasnicka, and J. Luitz, *WIEN2K, An Augmented Plane Wave + Local Orbitals Program for Calculating Crystal Properties*, Technische Universität Wien, Austria, 2001.

[49] J. P. Perdew, K. Burke, and M. Ernzerhof, Phys. Rev. Lett. **77**, 3865 (1996).

[50] S. L. Dudarev, G. A. Botton, S. Y. Savrasov, C. J. Humphreys, and A. P. Sutton, Phys. Rev. B **57**, 1505 (1998).

[51] M. T. Czyzyk and G. A. Sawatzky, Phys. Rev. B **49**, 14211 (1994).

[52] S. V. Streltsov, Phys. Rev. B **88**, 024429 (2013).

[53] H. J. Xiang, E. J. Kan, S.-H. Wei, M.-H. Whangbo, and X. G. Gong, Phys. Rev. B **84**, 224429 (2011).

[54] The reason for taking a ferromagnetic DOS is that it is the simplest magnetic configuration that tells us that the system is insulating upon inclusion of a Hubbard U.

[55] N. S. Fedorova, C. Ederer, N. A. Spaldin, and A. Scaramucci, Phys. Rev. B **91**, 165122 (2015).

[56] M. Kotani, J. Phys. Soc. Jpn. **4**, 293 (1949).

[57] H. Lu, J. R. Chamorro, C. Wan, and T. M. McQueen, Inorg. Chem. **57**, 14443 (2018).